Journal of Magnetism and Magnetic Materials 626 (2025) 173047

Contents lists available at ScienceDirect

Journal of Magnetism and Magnetic Materials

journal homepage: www.elsevier.com/locate/jmmm

Demagnetization factors and field of hemispherical objects

Frederik L. Durhuus [a], Ellen Fogh [a,b], Thomas Jauho [a], Marco Beleggia [c,d,*]

[a] Department of Physics, Technical University of Denmark, 2800 Kgs. Lyngby, Denmark
[b] Laboratory for Quantum Magnetism, Institute of Physics, École Polytechnique Fédérale de Lausanne (EPFL), CH-1015 Lausanne, Switzerland
[c] DTU Nanolab, Technical University of Denmark, 2800 Kgs. Lyngby, Denmark
[d] Department of Physics, University of Modena and Reggio Emilia, 41125 Modena, Italy

ARTICLE INFO

Keywords:
Demagnetization factor
Demagnetization field
Analytical magnetostatics
Shape amplitude
Shape anisotropy

ABSTRACT

Demagnetization factors play an important role in micromagnetics modeling but exact solutions only exist for a limited number of particle shapes. Here we use a Fourier space based approach coupled to the concept of magnetic charges to derive analytically the demagnetization factors for shapes that are subsets of a sphere: spherical sectors and spherical caps. For the uniformly magnetized hemisphere, which is a special case of both geometries, the exact demagnetization factors are shown to be $N_x = N_y = 7/(9\pi)$ parallel to the bottom plane and $N_z = 1 - 14/(9\pi)$ in the direction of the dome. Additionally, we provide expressions for shape amplitudes and demagnetization fields of these objects in terms of rapidly converging series. Our work demonstrates the potential of evaluating shape amplitudes to determine demagnetization factors in certain geometries and our results may facilitate numerical simulations of, for example, ferromagnetic droplets.

1. Introduction

The demagnetization factors, functions of the geometrical shape of a given body, are proportional to the magnetostatic energy density of the body itself, when it is uniformly magnetized. The computation of magnetostatic energies, by far the most difficult aspect of micromagnetics, is greatly simplified when demagnetization factors are known explicitly. For example the Magtense micromagnetics solver [1] relies on analytical solutions for the demagnetization field of a tetrahedron [2]. Also, analytical results on demagnetization effects are useful in testing and benchmarking such numerical software.

In presence of sufficiently strong applied magnetic field, large magnetocrystalline anisotropy, or in case of sufficiently small particles [3,4], the magnetization topography is well represented by a single uniform single-domain state. An example of a physical realization with hemispherical geometry is found in ferrofluid droplets on a flat surface in a uniform applied field [5–7]. In such cases, a number of exact, analytical expressions for demagnetization factors may be obtained for simple shapes: Maxwell gave the expression for bodies in the shape of ellipsoids of revolution [8,9], rectangular blocks were first solved by Rhodes and Rowlands [10,11], followed by blocks with triangular cross-section [12,13]; cylinders were discussed in Refs. [12,14,15] and more recently in Ref. [16,17]. The analytical results, particularly those for ellipsoidal and rectangular bodies, have been used extensively to elucidate the quantitative aspects of the geometry of domain structure [18].

Later the problem was worked out in a very general fashion by using Fourier-space techniques [19]. With this development, the class of exact solutions has become much broader. As it stands, the demagnetization-factor problem can be considered solved for all uniformly magnetized bodies, for which the corresponding shape amplitude is known [20]. Results originating from this development include the demagnetization factors of the elliptic cylinder [21], torus [22], ring with rectangular cross section [23] and cylindrical shell [24], as well as an alternative, more transparent and computationally advantageous solution for the ellipsoid [25].

In this paper, we extend the set of solved demagnetization problems to the hemisphere and related shapes. The present contribution will assist in developing, validating and benchmarking micromagnetics solvers; especially given recent interest in the magnetism of curved geometries [26], including solid spherical caps [27,28].

2. Problem and methods

We consider a uniformly magnetized hemispherical magnet of radius R, with saturation magnetization M_0 as well as spherical sectors and spherical caps (Fig. 1). We derive exact expressions for the demagnetization factors, N_x, N_y, N_z, for each shape, i.e. the eigenvalues of the demagnetization tensor N which connects the **M** and **H** fields by

$$H_i = -N_{ij} M_j \quad (i, j = x, y, z). \tag{1}$$

* Corresponding author at: Department of Physics, University of Modena and Reggio Emilia, 41125 Modena, Italy.
E-mail address: marco.beleggia@unimore.it (M. Beleggia).

https://doi.org/10.1016/j.jmmm.2025.173047
Received 10 May 2024; Received in revised form 21 March 2025; Accepted 7 April 2025
Available online 19 April 2025
0304-8853/© 2025 The Author(s). Published by Elsevier B.V. This is an open access article under the CC BY license (http://creativecommons.org/licenses/by/4.0/).

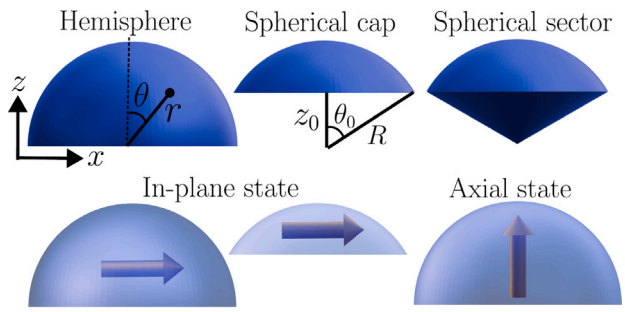

Fig. 1. Illustration of the shapes for which we calculate the demagnetization factors (top row), and the magnetization states for which we calculate the demagnetization field (bottom row). Arrows indicate magnetization direction. Cartesian and spherical coordinates are shown on the hemisphere, while radius R, opening angle θ_0, and cap height $z_0 = R\cos\theta_0$ are shown on the spherical cap. Note that we never use the Cartesian coordinates in calculations, but instead define $x = z/R = \cos\theta$ and $x_0 = z_0/R = \cos\theta_0$ to be consistent with standard notation for Legendre polynomials. The spherical cap and sector are drawn with an opening angle of $\theta_0 = 60°$, and the figures are to scale.

Given the eigenvalues, N can be expressed in any inertial reference frame by a standard coordinate transform. We also derive the demagnetization field with in-plane magnetization for the hemisphere and spherical cap, as well as for the axially magnetized hemisphere (Fig. 1).

Since for any uniformly magnetized shape the trace of the magnetometric demagnetization tensor is unity, meaning $N_x + N_y + N_z = 1$, and considering that $N_x = N_y$ by rotational symmetry, we only have to calculate one factor. We choose to compute N_z, the axial demagnetization factor, from the following expression [19]

$$N_z = \frac{1}{8\pi^3 V}\int \frac{\mathrm{d}^3\mathbf{k}}{k^2}|D(\mathbf{k})|^2 k_z^2, \tag{2}$$

where

$$D(\mathbf{k}) = \int_{\text{object}} \mathrm{e}^{-i\mathbf{k}\cdot\mathbf{r}}\mathrm{d}\mathbf{r} \tag{3}$$

is known as the shape amplitude or, in other words, the Fourier transform of the shape of an object.

As for the demagnetization field generated by the uniformly magnetized object, we recall that [29]

$$\mathbf{H}(\mathbf{r}) = -\frac{M_0}{8\pi^3}\int \frac{\mathrm{d}^3\mathbf{k}}{k^2} D(\mathbf{k})(\hat{\mathbf{m}}\cdot\mathbf{k})\mathbf{k}e^{i\mathbf{k}\cdot\mathbf{r}}, \tag{4}$$

where $\hat{\mathbf{m}} = \mathbf{M}/M_0$. Considering that $\nabla\times\mathbf{H} = 0$ so that $\mathbf{H} = -\nabla\varphi$, the computation reduces to evaluating the scalar potential, φ, which is given by

$$\varphi(\mathbf{r}) = -\frac{\mathrm{i}M_0}{8\pi^3}\int \frac{\mathrm{d}^3\mathbf{k}}{k^2} D(\mathbf{k})(\hat{\mathbf{m}}\cdot\mathbf{k})e^{i\mathbf{k}\cdot\mathbf{r}}, \tag{5}$$

as can be verified by substitution. For the hemisphere and spherical sector, we carry out the integrals in Eqs. (2)–(4) directly. However for the spherical cap we found it more expedient to use the notion of magnetic charges.

In the present context, the **H**-field and scalar potential bear a strong resemblance to the **E**-field and associated potential in electrostatics. In particular, since $\mathbf{H} = \mu_0^{-1}\mathbf{B} - \mathbf{M}$ we have

$$\boldsymbol{\nabla}\cdot\mathbf{H} = -\nabla^2\varphi = -\boldsymbol{\nabla}\cdot\mathbf{M} \tag{6}$$

so φ is governed by a Poisson equation and

$$\rho_m = -\boldsymbol{\nabla}\cdot\mathbf{M} \tag{7}$$

may be regarded as an effective volume charge density, which is identically zero when the magnetization is uniform. From Eq. (7) we can derive the density of magnetic surface charges, σ_m. Integrating Eq. (7) over an infinitesimally thin box containing a surface patch, it follows from Gauss theorem that

$$\sigma_m = (\mathbf{M}_{\text{in}} - \mathbf{M}_{\text{out}})\cdot\hat{\mathbf{n}} \tag{8}$$

where $\mathbf{M}_{\text{in}}$ ($\mathbf{M}_{\text{out}}$) is the magnetization right inside (outside) the surface and $\hat{\mathbf{n}}$ is an outward facing unit normal.

We can also develop an expression for N_i in terms of magnetic charges by comparing two expressions for the magnetostatic self-energy E_m, which is the work required to assemble a magnetization distribution against the dipole–dipole repulsion. Starting from Eq. D.12 in Ref. [30] we find that

$$\begin{aligned} E_m &= -\frac{\mu_0}{2}\int \mathbf{M}\cdot\mathbf{H}\mathrm{d}\mathbf{r} = \frac{\mu_0}{2}\int \mathbf{M}\cdot\nabla\varphi\mathrm{d}\mathbf{r} \\ &= \frac{\mu_0}{2}\int \varphi\boldsymbol{\nabla}\cdot\mathbf{M}\mathrm{d}\mathbf{r} = \frac{\mu_0}{2}\int \varphi\rho_m\mathrm{d}\mathbf{r}. \end{aligned} \tag{9}$$

That means that the energy in the demagnetization field is given by an integral over the scalar potential and magnetic charge density. This is completely analogous to the work required to assemble a collection of charges in electrostatics, see e.g. Sec. 2.4.3 in Ref. [31]. In Ref. [25] it was shown that

$$E_m = \frac{\mu_0 M_0^2 V}{2}(N_x\hat{m}_x^2 + N_y\hat{m}_y^2 + N_z\hat{m}_z^2) \tag{10}$$

also holds. By combining Eqs. (9) and (10) for a given magnetization we may calculate demagnetization factors directly from the demagnetization field, thus circumventing the shape amplitude. There are situations where this approach is particularly convenient.

3. Shape amplitudes

Here, as in the rest of the paper, we choose a spherical reference system conventionally oriented, with $\mathbf{r} = (r,\theta,\phi)$ and $\mathbf{k} = (k,\theta',\phi')$ in spherical coordinates (Fig. 1).

3.1. Spherical sector

The spherical sector is the intersection of a sphere with radius R and a cone with opening angle θ_0, so it has the spherical coordinates $(r,\theta,\phi) = (R, 0..\theta_0, 0..2\pi)$. Its shape amplitude is (see Eq. (3))

$$D(\mathbf{k}) = \int_0^R r^2\mathrm{d}r\int_0^{\theta_0}\sin\theta\mathrm{d}\theta\int_0^{2\pi}\mathrm{d}\phi\, e^{-i\mathbf{k}\cdot\mathbf{r}}. \tag{11}$$

Using the decomposition of a plane wave into spherical waves, commonly referred to as Rayleigh's expansion

$$e^{-i\mathbf{k}\cdot\mathbf{r}} = 4\pi\sum_{\ell=0}^{\infty}(-\mathrm{i})^\ell j_\ell(kr)\sum_{m=-\ell}^{\ell}(-1)^m Y_\ell^{-m}(\theta',\phi')Y_\ell^m(\theta,\phi), \tag{12}$$

where j_ℓ is a spherical Bessel function of the first kind, and

$$Y_\ell^m(\theta,\phi) = \sqrt{\frac{2\ell+1}{4\pi}\frac{(\ell-m)!}{(\ell+m)!}}P_\ell^m(\cos\theta)\mathrm{e}^{im\phi} \tag{13}$$

a spherical harmonic function with P_ℓ^m an associated Legendre polynomial. Writing out Eq. (12) in terms of P_ℓ^m yields

$$\begin{aligned} e^{-i\mathbf{k}\cdot\mathbf{r}} = \sum_{\ell=0}^{\infty}(-\mathrm{i})^\ell(2\ell+1)j_\ell(kr)\sum_{m=-\ell}^{\ell}(-1)^m\frac{(\ell-m)!}{(\ell+m)!} \\ \times P_\ell^m(\cos\theta')P_\ell^m(\cos\theta)e^{im(\phi-\phi')}. \end{aligned} \tag{14}$$

Integrating over ϕ, only the $m = 0$ terms remain and we obtain

$$\begin{aligned} D(\mathbf{k}) = 2\pi\sum_{\ell=0}^{\infty}(-\mathrm{i})^\ell(2\ell+1)P_\ell(\cos\theta') \\ \times\int_0^R r^2\mathrm{d}r j_\ell(kr)\int_{x_0}^1\mathrm{d}x P_\ell(x) \end{aligned} \tag{15}$$

where $x_0 = \cos\theta_0$ and we used the identity

$$\int_0^{\theta_0} P_\ell(\cos\theta)\sin\theta \mathrm{d}\theta = \int_{x_0}^{1} P_\ell(x)\mathrm{d}x\,. \tag{16}$$

We define the coefficient functions

$$a_\ell(x_0) = (2\ell+1)\int_{x_0}^{1} \mathrm{d}x P_\ell(x), \tag{17}$$

noting that $a_0(x_0) = 1 - x_0$ while for $\ell \geq 1$ it follows from $P_\ell(1) = 1$ and a known recurrence relation (Eq. (12.88) in Ref. [32]) that

$$a_\ell(x_0) = P_{\ell-1}(x_0) - P_{\ell+1}(x_0). \tag{18}$$

Next we define the auxiliary functions

$$F_\ell(k) = \int_0^R r^2 j_\ell(kr)\mathrm{d}r. \tag{19}$$

While F_ℓ can be expressed in terms of hypergeometrics, their explicit form is not particularly enlightening or useful so we keep them implicit.

With Eqs. (17) and (19), the shape amplitude for a spherical sector takes the simpler form

$$D(\mathbf{k}) = 2\pi \sum_{\ell=0}^{\infty} (-\mathrm{i})^\ell a_\ell(x_0) F_\ell(k) P_\ell(\cos\theta'). \tag{20}$$

3.2. Hemisphere

The hemisphere is the special case of a spherical sector where $\theta_0 = \pi/2$. In this case $x_0 = 0$ and Eq. (17) simplifies to

$$a_{2\ell}(0) = 0 \quad , \quad a_{2\ell-1}(0) = (-1)^{\ell+1}(4\ell-1)\frac{(2\ell-3)!!}{(2\ell)!!}, \tag{21}$$

for $\ell \geq 1$ while $a_0(0) = 1$. Thus for the hemisphere specifically, all terms where ℓ is even and non-zero vanish. For convenience we define

$$a_\ell = (-1)^{\ell+1} a_{2\ell-1}(0) \quad \text{and} \quad \alpha_\ell = \frac{a_\ell}{4\ell-1} = \frac{(2\ell-3)!!}{(2\ell)!!}. \tag{22}$$

From Eq. (20) we then arrive at

$$D(\mathbf{k}) = \frac{1}{2} D_S(k) - 2\pi\mathrm{i} \sum_{\ell=1}^{\infty} a_\ell F_{2\ell-1}(k) P_{2\ell-1}(\cos\theta') \tag{23}$$

with

$$D_S(k) = 4\pi R^2 j_1(kR)/k \tag{24}$$

the shape amplitude of the sphere.

In Fig. 2 we use Eqs. (20) and (23) to numerically compute the shape amplitude. We plot $|D(\mathbf{k})|$ since this is the relevant quantity for demagnetization factors (*cf.* Eq. (2)). This essentially produces a Fourier space representation of the shape. For the sphere, rotational symmetry is retained, but we observe secondary rings around the center. The $\theta_0 = 3\pi/4$ spherical sector is shorter in the z-direction, hence elongated along the k_z-axis and giving the impression of a rounded rectangle. The hemisphere is more oblong still, and the $\pi/4$-sector is the most diffuse in k-space due to its smaller size in real-space.

4. Demagnetization fields

4.1. Hemisphere: axial state

With the shape amplitude written down, we can calculate the demagnetization field generated by the hemisphere inside and outside from Eqs. (4) and (5). Inserting $\hat{\mathbf{m}} \cdot \mathbf{k} = k_z = k\cos\theta'$ in Eq. (5) for axial magnetization, using the complex conjugate of Eq. (14) for the exponential and integrating over ϕ', we have

$$\varphi = -\frac{\mathrm{i}M_0}{4\pi^2} \sum_{\ell=0}^{\infty} \mathrm{i}^\ell (2\ell+1) P_\ell(\cos\theta) \times \int_0^\infty k\mathrm{d}k\, j_\ell(kr) \int_{-1}^{1} x\mathrm{d}x\, P_\ell(x) D(k,x) \tag{25}$$

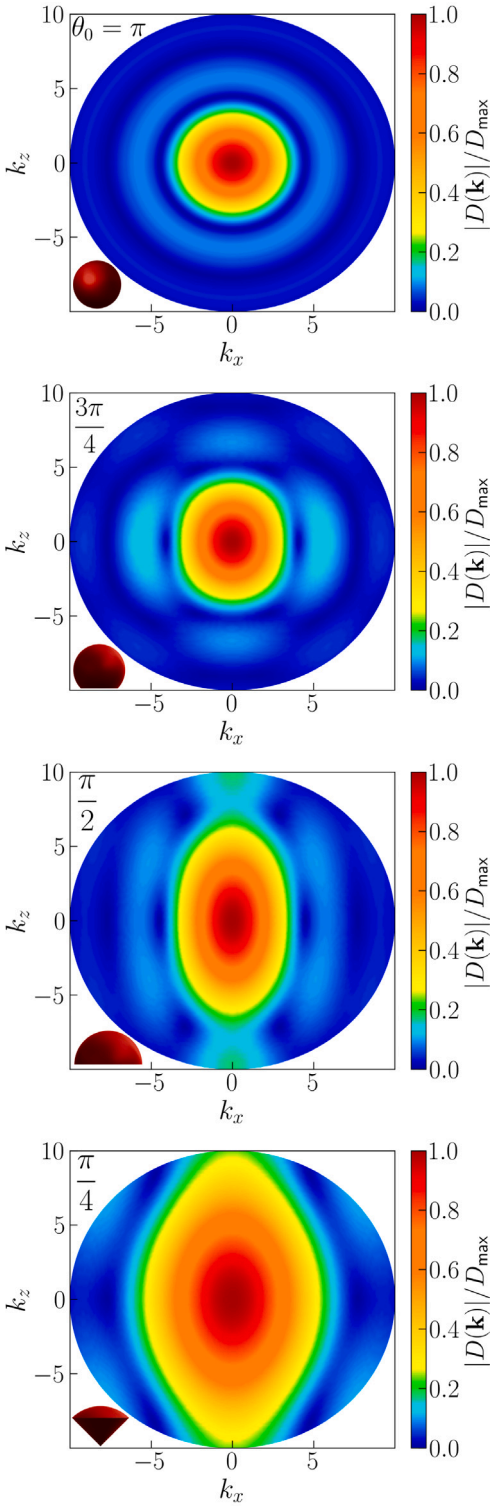

Fig. 2. Absolute value of the shape amplitude for different spherical sectors, including sphere and hemisphere, computed using Eqs. (20) and (23). The opening angle θ_0 is shown in the top-left corner and a side-view of the geometry in the bottom-left. The colorscale is normalized to the highest value of $|D|$ for each shape.

with $x = \cos\theta'$. Since $D(k,x)$ has split into a real and an imaginary part, we compute the two parts separately. We obtain $\varphi = \varphi_d + \varphi_h$, where (see Appendix A for intermediate steps):

$$\varphi_d = \frac{mz}{4\pi} \begin{cases} 1/R^3 & \text{for} \quad r \leq R \\ 1/r^3 & \text{for} \quad r \geq R \end{cases} \tag{26}$$

i.e. the dipole potential ($m = 2\pi R^3 M_0/3$ is the hemisphere's dipole moment), and the final expressions for the φ_h potential in the two regions $r > R$ and $r < R$ are

$$\varphi_h(r \geq R) = -\frac{3m}{4\pi}\sum_{\ell=1}^{\infty}(-1)^\ell \alpha_\ell \frac{\ell}{\ell+1} P_{2\ell}(\cos\theta)\frac{R^{2\ell-1}}{r^{2\ell+1}} \tag{27}$$

and

$$\varphi_h(r \leq R) = -\frac{3m}{4\pi}\sum_{\ell=1}^{\infty}(-1)^\ell \alpha_\ell \left[\frac{\ell}{\ell+1} P_{2\ell}(\cos\theta) - \frac{2\ell-1}{2\ell-3} P_{2\ell-2}(\cos\theta)\left(1-\frac{r^{2\ell-3}}{R^{2\ell-3}}\right)\right]\frac{r}{R^3}, \tag{28}$$

with α_ℓ defined in Eq. (22). We note that $\varphi_h(r < R)$ can be simplified by reindexing $\ell \to \ell+1$ in the second part and using that $\alpha_{\ell+1} = \frac{2\ell-1}{2\ell+2}\alpha_\ell$. Introducing $\varphi_0 = m/(4\pi R^2) = M_0 R/6$, the rescaled radius $\rho = r/R$ and a new set of coefficients $\beta_\ell = (-1)^\ell \alpha_\ell/(\ell+1)$, we can thus write the normalized magnetic potential $\bar{\varphi} = \varphi/\varphi_0$ as

$$\bar{\varphi}(\rho \geq 1) = \frac{\cos\theta}{\rho^2} - 3\sum_{l=1}^{\infty}\frac{\ell\,\beta_\ell}{\rho^{2\ell+1}} P_{2\ell}(\cos\theta) \tag{29}$$

$$\bar{\varphi}(\rho \leq 1) = \rho\cos\theta - \frac{3}{2}\sum_{l=0}^{\infty}\beta_\ell\left[(4\ell+1)\rho - (2\ell+1)\rho^{2\ell}\right]P_{2\ell}(\cos\theta) \tag{30}$$

Note that the potential is continuous across the two regions at $\rho = 1$; its value at $\rho = 0$ (center of the hemisphere's bottom surface and south pole) is $-3/2$, while at $\rho = 1$, $\theta = 0$ (north pole) is $3 - \sqrt{2} \approx 1.586$. Note also that the electric potential of a uniformly polarized hemisphere coincides with the magnetic scalar potential just obtained with the substitutions $m \to p$ (magnetic moment into electric dipole moment) and $\varphi_0 \to V_0 = p/(4\pi\epsilon_0 R^2) = P_0 R/(6\epsilon_0)$, where P_0 is electric polarization density.

4.2. Hemisphere: in-plane state

When the magnetization points along the x-axis, $\mathbf{k}\cdot\hat{\mathbf{m}} = k_x$ in the scalar potential (Eq. (5)). Since $k_x = k\cos\phi'\sin\theta'$, we break the azimuthal symmetry and, seemingly, complicate things. However, looking ahead, the in-plane state implies the absence of magnetic charges on the circular bottom surface of the hemisphere, so that, in the end, both the potential and the demagnetization factors are going to be less cumbersome than for the axial state.

Like the axial case, we use Rayleigh's expansion, Eq. (14), but due to the extra $\cos\phi'$ originating from k_x, we use the identity

$$\int_0^{2\pi}\cos\phi' \mathrm{d}\phi' e^{im\phi'} = \pi(\delta_{m,1} + \delta_{m,-1}) \tag{31}$$

for the azimuthal integration. Furthermore, since $\sin\theta' = -P_1^1(\cos\theta')$, and

$$P_\ell^{-m} = (-1)^m\frac{(\ell-m)!}{(\ell+m)!}P_\ell^m, \tag{32}$$

the potential for in-plane polarization φ^x may be written

$$\varphi^x = \frac{iM_0}{4\pi^2}\cos\phi\sum_{n=1}^{\infty} i^n\frac{2n+1}{n(n+1)}P_n^1(\cos\theta) \times \int_0^\infty k\mathrm{d}k\, j_n(kr)\int_{-1}^{1}\mathrm{d}x\, P_1^1(x)P_n^1(x)D(k,x). \tag{33}$$

Once more (see Appendix A for intermediate steps), the $1/(2D_S(k))$ term in $D(k,x)$ generates a dipole potential

$$\varphi_d^x = \frac{mx}{4\pi}\begin{cases} 1/R^3 & \text{for} \quad r \leq R \\ 1/r^3 & \text{for} \quad r \geq R \end{cases} \tag{34}$$

only now oriented along x. After adding φ_h^x and non-dimensionalizing as in the axial case (see Appendix A), the result is:

$$\bar{\varphi}^x(\rho \leq 1) = \rho\cos\phi\sin\theta + \frac{3}{2}\cos\phi\sum_{\ell=1}^{\infty}\beta_\ell\rho^{2\ell}P_{2\ell}^1(\cos\theta) \tag{35}$$

$$\bar{\varphi}^x(\rho \geq 1) = \frac{\cos\phi\sin\theta}{\rho^2} + \frac{3}{2}\cos\phi\sum_{\ell=1}^{\infty}\frac{\beta_\ell}{\rho^{2\ell+1}}P_{2\ell}^1(\cos\theta). \tag{36}$$

4.3. Spherical cap: in-plane state

The spherical cap is essentially the spherical sector without the conical part. The shape amplitude calculation is difficult for this shape, so instead we use magnetic charges to calculate the scalar potential. From Eqs. (6) and (8) it is seen that $\rho_m = 0$, while $\sigma_m = M_0\sin\theta\cos\phi$ on the curved top and zero on the bottom plane. Hence we have the boundary-value problem

$$\nabla^2\varphi = 0 \quad , \quad \partial_r\varphi\Big|_{r=R,\theta\leq\theta_0} = M_0\sin\theta\cos\phi. \tag{37}$$

We solve Eq. (37) in Appendix A.3, finding that

$$\varphi^x = \frac{M_0R^2}{2}\cos\phi\sum_{\ell=1}^{\infty}\frac{r_<^\ell}{r_>^{\ell+1}}\gamma_\ell(x_0)P_\ell^1(\cos\theta) \tag{38}$$

where $r_< = \min(r,R)$ and $r_> = \max(r,R)$, and the coefficients are

$$\gamma_\ell(x_0) = \frac{1}{2\ell+1}\left[\frac{P_\ell(x_0)-P_{\ell-2}(x_0)}{2\ell-1} - \frac{P_{\ell+2}(x_0)-P_\ell(x_0)}{2\ell+3}\right] \tag{39}$$

for $\ell \geq 2$ while $\gamma_1(x_0) = (3x_0 - 2 - x_0^3)/6$.

We note that in the special case of a hemisphere ($\theta_0 = \pi/2 \to x_0 = 0$) we have $\gamma_{2\ell+1} = 0$ for $\ell \geq 1$ while $\gamma_1 = -1/3$ and $\gamma_{2\ell} = \beta_\ell/2$. Inserting in Eq. (38) reproduces the potential in Section 4.2 as it should.

In Fig. 3 we use the results of Sections 4.1, 4.2 and 5.3 to compute the normalized scalar potential. Since $\mathbf{H} = -\boldsymbol{\nabla}\varphi$ the field-lines of the demagnetization field go from positive potential (red) to negative potential (blue), so the plots indicate the demagnetization field structure as well.

In every case with in-plane magnetization, there is mirror symmetry through a vertical, zero-potential plane at $x = 0$. There is a compact region with positive magnetic charge (positive potential) at $x > 0$ and negative charge at $x < 0$, suggesting a nearly dipolar field outside. However, we note that the magnitude of the potential is greater on the curved, upper part because this is the location of magnetic charges. This gives an asymmetric field which is stronger on the top-part than bottom.

For the axially magnetized hemisphere (bottom plot), the zero-potential contour is curved upwards, both inside and outside the hemisphere. This is because the positive and negative potential regions are asymmetric, since the positive magnetic charges are spread on a curved surface and the negative ones on a flat surface.

5. Demagnetization factors

As noted previously, for determining the demagnetization tensor, N, for the shapes of interest, it is sufficient to calculate one demagnetization factor since $N_x = N_y$ by symmetry and $N_x + N_y + N_z = 1$ for uniformly magnetized objects.

5.1. Hemisphere

We consider the axial demagnetization factor N_z, given in Eq. (2), which involves the square modulus of the shape amplitude. Re-examining Eq. (23), we note that it has separated into a real part, equal to half the shape amplitude of the sphere, and an imaginary part, featuring an infinite series. Its square modulus is then

$$|D(\mathbf{k})|^2 = |\mathrm{Re} - i\,\mathrm{Im}|^2 = \frac{1}{4}D_S(k)^2 + 4\pi^2 S^2(k,x) \tag{40}$$

where

$$S(k,x) = \sum_{\ell=1}^{\infty}a_\ell P_{2\ell-1}(x)F_{2\ell-1}(k) = \sum_{\ell=1}^{\infty}S_\ell. \tag{41}$$

The first term yields half the demagnetization factor of a sphere, since the prefactor is 1/4 but the volume V is half that of a sphere,

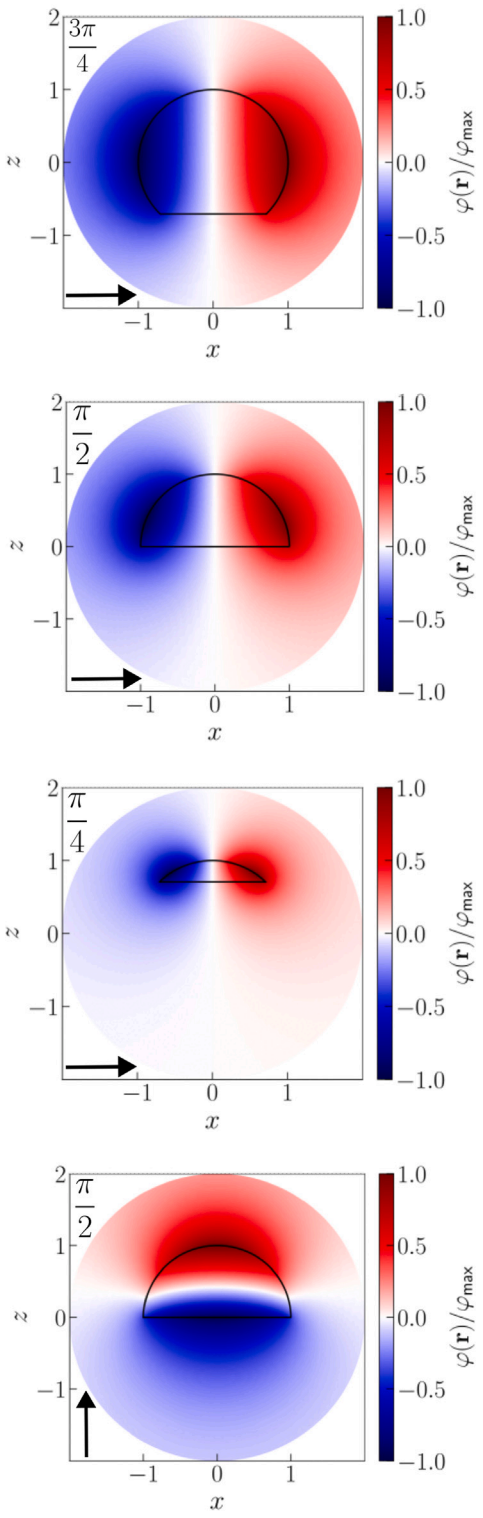

Fig. 3. Magnetic scalar potential for spherical caps and hemispheres, normalized to its maximal value. Shape outlines are drawn on top with arrows for magnetization direction and opening angle θ_0 indicated in the bottom and top left corners, respectively.

and the demagnetization factor for a sphere is 1/3. Thus the integral reduces to

$$N_z = \frac{1}{6} + \frac{3}{2\pi R^3}\int_0^\infty k^2 \mathrm{d}k \int_{-1}^{1} x^2 S^2(k,x)\mathrm{d}x \tag{42}$$

In Appendix B.1 we evaluate the rest of the expression. The final result is

$$N_z = \frac{1}{6} + \frac{1}{4}\sum_{\ell=1}^{\infty} b_\ell + \frac{1}{8}\sum_{\ell=1}^{\infty}\frac{2\ell-1}{\ell+1}c_\ell. \tag{43}$$

with the coefficients given in Eqs. (B.5) and (B.6). The series evaluates to $N_z = 1 - 14/(9\pi) = 0.504851$, so that the other two demagnetization factors are $N_x = N_y = 7/(9\pi) = 0.247574$.

5.2. Spherical sector

For the spherical sector we insert Eq. (20) into Eq. (2) to obtain

$$N_z(x_0) = \frac{1}{V}\int_0^\infty k^2\mathrm{d}k \int_{-1}^{1} x^2\mathrm{d}x \sum_{n,m=0}^{\infty} \mathrm{i}^{m-n} a_n(x_0) \times a_m(x_0) F_n(k) F_m(k) P_n(x) P_m(x). \tag{44}$$

We evaluate the expression in Appendix B.2, eventually finding that

$$N_z(x_0) = \frac{1}{4(1-x_0)}\sum_{n=0}^{\infty}\left[p_n(x_0) - \frac{2n}{n+3}q_n(x_0)\right]. \tag{45}$$

where p_n and q_n are found in Eqs. (B.14) and (B.15).

We note that when $x_0 = -1$ (sphere) $q_n = 0$ and $p_n = 8/3\delta_{n,0}$, so that $N_z(-1) = 1/3$ as expected.

5.3. Spherical cap

For the spherical cap, we calculate the in-plane demagnetization factor, N_x, from the in-plane magnetized state $\mathbf{M} = M_0\mathbf{e}_x$. From Eqs. (9) and (10) we then have

$$N_x = \frac{1}{M_0^2 V_{\mathrm{cap}}(\theta_0)}\int \varphi^x \rho_m \mathrm{d}\mathbf{r}. \tag{46}$$

We evaluate the cap volume and integral in Appendix B.3, finding that

$$N_x = \frac{3}{2(1-x_0)^2(2+x_0)}\sum_{\ell=1}^{\infty}\ell(\ell+1)\gamma_\ell^2(x_0), \tag{47}$$

with γ_ℓ defined in Eq. (39). In the limit $\theta_0 \to \pi$ (sphere) we have $\gamma_\ell(-1) = -(2/3)\delta_{\ell,1}$ so that $N_x = 1/3$ hence $N_y = N_z = 1/3$ as they should. In the limit $\theta_0 \to \pi/2$ (hemisphere) we find after some algebra (see Appendix B.3) that $N_x = N_y = 7/(9\pi)$ so that $N_z = 1 - 14/(9\pi)$ just like we found in Section 5.1.

In Fig. 4 we plot demagnetization factors for the shapes shown in Fig. 1 as function of opening angle, in addition to the sphere for comparison. We see that the spherical cap and sector both converge to the sphere for $\theta_0 = \pi$ and the hemisphere for $\theta_0 = \pi/2$, as they should. For $\theta_0 \geq \pi/2$ the cap and sector are nearly equal, because the only difference is that the cap is flat on the bottom while the sector curves inwards. In the opposite limit, $\theta_0 \to 0$, the sector becomes long and narrow, approaching $N_x = 0.5, N_z = 0$ just like a very thin cylindrical rod. Meanwhile the cap becomes flat, approaching the $N_x = 0, N_z = 1$ result of a flat plate. Finally, we note that the hemisphere has a greater axial factor and lower in-plane factor than the sphere, which is simply because a hemisphere is flatter than a sphere of equal volume. It is worth highlighting that the demagnetization factors for the spherical sector are non-monotonic in the opening angle. The N_z of the spherical sector reaches a maximum of ~0.58 at an opening angle of ~ 70°. Furthermore, rather surprisingly, a spherical sector with opening angle of ~ 25° is isotropic, having all demagnetization factors equal to 1/3.

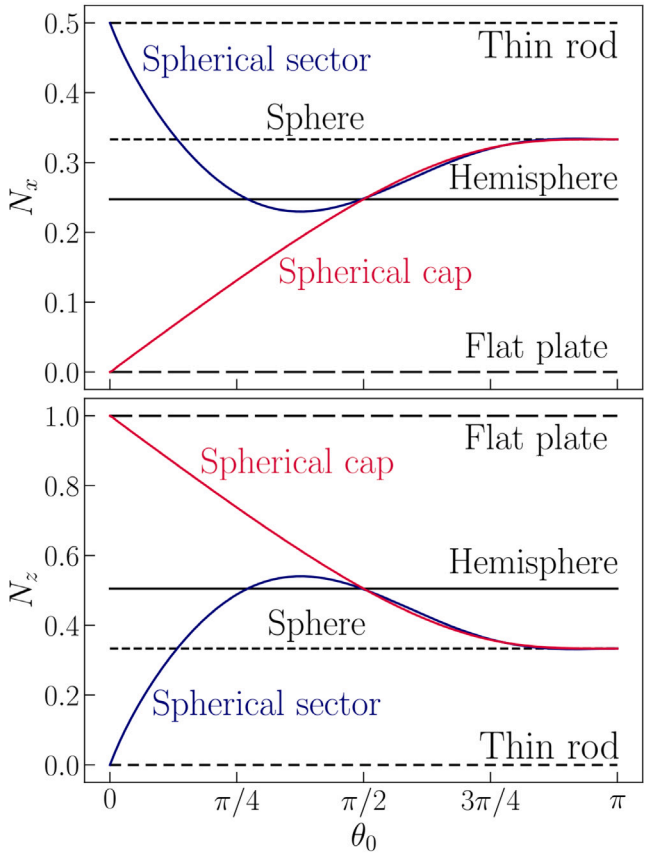

Fig. 4. Demagnetization factors, N_x (top) and N_z (bottom), for spherical cap (red curve) and spherical sector (blue curve) as a function of the opening angle, θ_0 compared with the hemisphere (solid black line) as well as sphere, thin rod and flat plate (dashed black lines).

6. Conclusion

By evaluating and integrating the shape amplitude following the Fourier approach, we determined the demagnetization factors of the general spherical sector in terms of a rapidly converging series. Using the complementary method of analyzing magnetic charges, we determined the magnetic scalar potential and the demagnetization factor for the general spherical cap, again in terms of infinite series. For both shapes, the hemisphere is a special case where the infinite series can be summed exactly, yielding $N_x = N_y = 7/(9\pi)$ for the in-plane demagnetization factors and $N_z = 1-14/(9\pi)$ for the axial factor. These exact results may facilitate future analytical and numerical modeling of micromagnetic systems.

CRediT authorship contribution statement

Frederik L. Durhuus: Writing – review & editing, Writing – original draft, Visualization, Methodology, Investigation, Formal analysis. **Ellen Fogh:** Writing – review & editing, Visualization, Methodology, Investigation, Formal analysis. **Thomas Jauho:** Methodology, Investigation, Formal analysis. **Marco Beleggia:** Writing – review & editing, Writing – original draft, Supervision, Methodology, Investigation, Formal analysis, Conceptualization.

Declaration of competing interest

The authors declare that they have no known competing financial interests or personal relationships that could have appeared to influence the work reported in this paper.

Appendix A. Scalar potential evaluation

A.1. Hemisphere: Axial magnetization

Here we calculate the scalar potential $\varphi = \varphi_d + \varphi_h$ for the axially polarized hemisphere, where φ_d results from the real part of the shape amplitude (first term in Eq. (23)) and φ_h from the imaginary part (rest of Eq. (23)).

Inserting in Eq. (25) we find that

$$\varphi_d = -\frac{iM_0R^2}{2\pi}\sum_{n=0}^{\infty} i^n(2n+1)P_n(\cos\theta) \times \int_0^\infty j_n(kr)j_1(kR)\mathrm{d}k \int_{-1}^{1} xP_n(x)\mathrm{d}x. \tag{A.1}$$

Since $x = P_1(x)$, it follows from the orthogonality of Legendre polynomials that

$$\varphi_d = \frac{M_0R^2}{\pi}\cos\theta \int_0^\infty j_1(kr)j_1(kR)\mathrm{d}k \tag{A.2}$$

The remaining integral is a special case of Eq. (4.13) in Ref. [33], but can also be derived from Eq. (1) in Ref. [34] using the relation

$$j_n(x) = \sqrt{\frac{\pi}{2x}}J_{n+1/2}(x) \tag{A.3}$$

between spherical- and regular Bessel functions of the first kind. The result is

$$\int_0^\infty j_1(kr)j_1(kR)\mathrm{d}k = \frac{\pi}{6}\begin{cases} r/R^2 & \text{for} \quad r<R \\ R/r^2 & \text{for} \quad r>R \end{cases} \tag{A.4}$$

which yields Eq. (26).

This leaves φ_h, which is given by

$$\varphi_h = -\frac{M_0}{2\pi}\sum_{n=0}^{\infty} \mathrm{i}^n(2n+1)P_n(\cos\theta) \times \int_0^\infty k\mathrm{d}k j_n(kr)\int_{-1}^{1} x\mathrm{d}x\, S(k,x)P_n(x) \tag{A.5}$$

where

$$S(k,x) = \sum_{\ell=1}^{\infty}(4\ell-1)\alpha_\ell F_{2\ell-1}(k)P_{2\ell-1}(x) \tag{A.6}$$

is the series in Eq. (23). Using the identity

$$\int_{-1}^{1} x\mathrm{d}x P_n(x)P_{n+1}(x) = \frac{(2n+2)}{(2n+1)(2n+3)}, \tag{A.7}$$

which follows from Bonnet's recursion formula and orthogonality, the integration along x gives

$$(4\ell-1)\int_{-1}^{1} x\mathrm{d}x\, P_{2\ell-1}(x)P_n(x) = \frac{4\ell}{4\ell+1}\delta_{n,2\ell} + \frac{4\ell-2}{4\ell-3}\delta_{n,2\ell-2} \tag{A.8}$$

so that we split φ_h further into two parts:

$$\varphi_h = -\frac{M_0}{\pi}\sum_{\ell=1}^{\infty}(-1)^\ell\alpha_\ell\int_0^\infty k\mathrm{d}k\int_0^R r'^2 j_{2\ell-1}(kr')\mathrm{d}r' \times [2\ell j_{2\ell}(kr)P_{2\ell}(\cos\theta) - (2\ell-1)j_{2\ell-2}(kr)P_{2\ell-2}(\cos\theta)]. \tag{A.9}$$

To carry out the integration in k, we use the transform in Eq. (A.3) and Eq. (6) in Ref. [34] to find that

$$\int_0^\infty k\mathrm{d}k j_{2\ell-1}(kr')j_{2\ell}(kr) = \frac{\pi}{2}\frac{r'^{2\ell-1}}{r^{2\ell+1}}\Theta(r-r') \tag{A.10}$$

and

$$\int_0^\infty k\mathrm{d}k j_{2\ell-1}(kr')j_{2\ell-2}(kr) = \frac{\pi}{2}\frac{r^{2\ell-2}}{r'^{2\ell}}\Theta(r'-r) \tag{A.11}$$

We can then straightforwardly integrate along r' to get the final expression for φ_h stated in Section 4.1.

A.2. Hemisphere: In-plane magnetization

Dividing the hemisphere shape factor, Eq. (23), in a real and an imaginary part and inserting in Eq. (33) for the in-plane potential, we get $\varphi^x = \varphi^x_d + \varphi^x_h$ where

$$\varphi^x_d = \frac{iM_0R^2}{2\pi}\cos\phi\sum_{n=1}^{\infty}\frac{i^n(2n+1)}{n(n+1)} \times\int_0^\infty j_n(kr)j_1(kR)\mathrm{d}k P^1_n(\cos\theta)\underbrace{\int_{-1}^{1}P^1_1(x)P^1_n(x)\mathrm{d}x}_{\frac{4}{3}\delta_{n,1}} = \frac{M_0R^2}{\pi}\sin\theta\cos\phi\int_0^\infty j_1(kr)j_1(kR)\mathrm{d}k. \tag{A.12}$$

Using Eq. (A.4), this yields Eq. (34).

The remaining portion of the calculation is

$$\varphi^x_h = \frac{M_0}{2\pi}\cos\phi\sum_{n=1}^{\infty}\mathrm{i}^n\frac{2n+1}{n(n+1)}P^1_n(\cos\theta) \times\int_0^\infty k\mathrm{d}k j_n(kr)\int_{-1}^{1}\mathrm{d}x P^1_1(x)P^1_n(x)S(k,x). \tag{A.13}$$

When expanding $S(k,x)$ we are left with integrals of the form

$$\int_{-1}^{1}\mathrm{d}x P^1_1(x)P^1_n(x)P^0_{2\ell-1}(x). \tag{A.14}$$

A more general version of this integral was studied by Infeld and Hull (Section 9.3 in Ref. [35], note that they normalized P such that $P^m_\ell\big|_{\text{I\&H}} = \sqrt{\frac{(2l+1)(l-m)!}{2(l+m)!}}P^m_\ell$ and in their notation $Y^m_\ell\big|_{\text{I\&H}} = \sin\theta\ P^m_\ell\big|_{\text{I\&H}}$). Using the various selection rules, the integral is zero unless $n = 2\ell$ or $n = 2\ell-2$ and evaluating both cases with Eq. (9.3.9) in Ref. [35] we get that

$$\frac{2n+1}{n(n+1)}\int_{-1}^{1}\mathrm{d}x P^1_1(x)P^1_n(x)P^0_{2\ell-1}(x) = \frac{2}{4\ell-1}\left(\delta_{n,2\ell}-\delta_{n,2\ell-2}\right). \tag{A.15}$$

It follows that

$$\varphi^x_h = \frac{M_0}{\pi}\cos\phi\sum_{\ell=1}^{\infty}(-1)^\ell\alpha_\ell\int_0^\infty k\mathrm{d}k\int_0^R r'^2 j_{2\ell-1}(kr')\mathrm{d}r' \times\left[P^1_{2\ell}(\cos\theta)j_{2\ell}(kr)+P^1_{2\ell-2}(\cos\theta)j_{2\ell-2}(kr)\right] \tag{A.16}$$

We have already handled the k-integrals in Appendix A.1. Inserting, integrating over r', adding φ^x_d and non-dimensionalizing as in the axial case, we get the $\bar{\varphi}^x_m$ expression in Section 4.2.

A.3. Spherical cap: In-plane magnetization

Consider the boundary value problem, Eq. (37). The general solution to the Laplace equation, $\nabla^2\varphi = 0$, in spherical coordinates is (see e.g. Eq. (3.61) in Ref. [36])

$$\varphi(r,\theta,\phi) = \sum_{\ell=0}^{\infty}\sum_{m=-\ell}^{\ell}[A_{\ell m}r^\ell + B_{\ell m}r^{-(\ell+1)}]Y^m_\ell(\theta,\phi) \tag{A.17}$$

where the spherical harmonic Y^m_ℓ is given in Eq. (13). First we divide the potential into an inside part i.e. $\varphi^{\text{in}}_m = \varphi(r\le R)$ and outside $\varphi^{\text{out}}_m = \varphi(r\ge R)$. To prevent divergence we require $B_{\ell m} = 0$ for φ^{in}_m and $A_{\ell m} = 0$ for φ^{out}. The potential is continuous at the cap surface, necessitating $B_{\ell m} = R^{2\ell+1}A_{\ell m}$, but the surface charge produces a discontinuity in the gradient:

$$\partial_r\varphi^{\text{in}}(r=R) - \partial_r\varphi^{\text{out}}(r=R) = \sigma_m \tag{A.18}$$

This boundary condition amounts to

$$\sum_{\ell=1}^{\infty}\sum_{m=-\ell}^{\ell}(2\ell+1)A_{\ell m}R^{\ell-1}Y^m_\ell(\theta,\phi) = M_0\Theta(\theta_0-\theta)\cos\phi\sin\theta \tag{A.19}$$

It follows from the orthogonality of spherical harmonics that

$$A_{\ell m} = \frac{M_0}{(2\ell+1)R^{\ell-1}}\int_0^{2\pi}\cos\phi\mathrm{d}\phi\int_0^{\theta_0}\sin^2\theta\mathrm{d}\theta Y^m_\ell(\theta,\phi) \tag{A.20}$$

From the ϕ-integration the only non vanishing terms are for $m=\pm1$. Using Eq. (32) we can write

$$A_{\ell,\pm1} = \mp\frac{M_0}{R^{\ell-1}}\sqrt{\frac{\pi(\ell+1)!}{4(2\ell+1)(\ell-1)!}}\int_{x_0}^{1}\sqrt{1-x^2}P^{-1}_\ell(x)\mathrm{d}x. \tag{A.21}$$

To carry out the x-integral, we use the recurrence relation, Eq. (12.86) in Ref. [32]

$$(2\ell+1)\sqrt{1-x^2}P^m_\ell = (P^{m+1}_{\ell-1}-P^{m+1}_{\ell+1}) \tag{A.22}$$

and Eqs. (17) and (18) to find that

$$\int_{x_0}^{1}\sqrt{1-x^2}P^{-1}_\ell(x)\mathrm{d}x = \frac{1}{2\ell+1}\left[\frac{a_{\ell-1}(x_0)}{2\ell-1}-\frac{a_{\ell+1}(x_0)}{2\ell+3}\right] = \frac{1}{2\ell+1}\left[\frac{P_{\ell-2}(x_0)-P_\ell(x_0)}{2\ell-1}-\frac{P_\ell(x_0)-P_{\ell+2}(x_0)}{2\ell+3}\right]. \tag{A.23}$$

for $\ell\ge2$, while in the special case of $\ell=1$

$$\int_{x_0}^{1}\sqrt{1-x^2}P^{-1}_1(x)\mathrm{d}x = \frac{1}{3}-\frac{1}{2}x_0+\frac{1}{6}x_0^3. \tag{A.24}$$

Inserting in Eq. (A.17) gives the potential expressed in Eq. (38).

Appendix B. Demagnetization factor calculations

B.1. Hemisphere

Here we evaluate the axial demagnetization factor of the hemisphere, starting from Eq. (42). The square of an infinite series involves the sum of each term squared, plus twice the sum of any two terms:

$$S^2 = (S_1+S_2+S_3+\cdots)^2 = \sum_{\ell=1}^{\infty}S^2_\ell + 2\sum_{\ell=1}^{\infty}S_\ell S_{\ell+1} + 2\sum_{\ell=1}^{\infty}S_\ell S_{\ell+2}+\cdots \tag{B.1}$$

Now, using Bonnet's recursion formula twice, one may show that

$$\int_{-1}^{1}x^2P_\ell(x)P_{\ell'}(x)\mathrm{d}x = \begin{cases}\frac{2(\ell+1)(\ell+2)}{(2\ell+1)(2\ell+3)(2\ell+5)} & \text{for}\quad \ell'=\ell+2\\ \frac{2(2\ell^2+2\ell-1)}{(2\ell-1)(2\ell+1)(2\ell+3)} & \text{for}\quad \ell'=\ell\\ \frac{2\ell(\ell-1)}{(2\ell-3)(2\ell-1)(2\ell+1)} & \text{for}\quad \ell'=\ell-2\end{cases} \tag{B.2}$$

and the integral is 0 for all other ℓ,ℓ' combinations. Thus, the only non-vanishing terms are

$$S^2_\ell = \sum_{\ell=1}^{\infty}a^2_\ell F^2_{2\ell-1}(k)\int_{-1}^{1}x^2P^2_{2\ell-1}(x)\mathrm{d}x = \sum_{\ell=1}^{\infty}b_\ell F^2_{2\ell-1}(k) \tag{B.3}$$

and

$$S_\ell S_{\ell+1} = 2\sum_{\ell=1}^{\infty}a_\ell a_{\ell+1}F_{2\ell-1}(k)F_{2\ell+1}(k) \times\int_{-1}^{1}x^2P_{2\ell-1}(x)P_{2\ell+1}(x)\mathrm{d}x = \sum_{\ell=1}^{\infty}c_\ell F_{2\ell-1}(k)F_{2\ell+1}(k) \tag{B.4}$$

where

$$b_\ell = a^2_\ell\frac{2(8\ell^2-4\ell-1)}{(4\ell-3)(4\ell-1)(4\ell+1)} \tag{B.5}$$

and

$$c_\ell = a_\ell a_{\ell+1}\frac{4\ell(2\ell+1)}{(4\ell-1)(4\ell+1)(4\ell+3)}. \tag{B.6}$$

We are then left with the radial integrals. Using the orthogonality of spherical Bessel functions

$$\int_0^\infty k^2 \mathrm{d}k j_\ell(kr) j_\ell(k\rho) = \frac{\pi}{2r^2}\delta(\rho - r) \tag{B.7}$$

we find that

$$\int_0^\infty F_{2\ell-1}^2(k)\mathrm{d}k = \int_0^R r^2\mathrm{d}r \int_0^R r'^2\mathrm{d}r' \frac{\pi}{2r^2}\delta(r-r') = \frac{\pi R^3}{6} \tag{B.8}$$

The demagnetization factor at this stage is therefore

$$N_z = \frac{1}{6} + \frac{1}{4}\sum_{\ell=1}^\infty b_\ell + \frac{3}{2\pi R^3}\sum_{\ell=1}^\infty c_\ell \int_0^\infty k^2 \mathrm{d}k F_{2\ell-1}(k) F_{2\ell+1}(k) \tag{B.9}$$

To evaluate the remaining integral we use the recursive relationship between spherical Bessel functions

$$j_{\ell+1}(x) = (2\ell+1)j_\ell(x)/x - j_{\ell-1}(x) \tag{B.10}$$

and the Bessel integrals presented in Appendix A.1 to obtain

$$\begin{aligned}\int_0^\infty k^2 \mathrm{d}k j_{2\ell-1}(kr') j_{2\ell+1}(kr) &= \frac{4\ell+1}{r}\int_0^\infty k\mathrm{d}k \\ &\times j_{2\ell-1}(kr')j_{2\ell}(kr) - \int_0^\infty k^2\mathrm{d}k j_{2\ell-1}(kr')j_{2\ell-1}(kr) \\ &= \frac{\pi}{2}(4\ell+1)\frac{r'^{2\ell-1}}{r^{2\ell+2}}\Theta(r-r') - \frac{\pi}{2r^2}\delta(r-r').\end{aligned} \tag{B.11}$$

Thus

$$\begin{aligned}\int_0^\infty k^2\mathrm{d}k F_{2\ell-1}(k)F_{2\ell+1}(k) &= \frac{\pi}{12}\frac{4\ell+1}{\ell+1}R^3 - \frac{\pi R^3}{6} \\ &= \frac{\pi}{6}R^3\frac{2\ell-1}{2(\ell+1)}.\end{aligned} \tag{B.12}$$

Inserting in Eq. (B.9) gives the final expression for the demagnetization factor Eq. (43).

B.2. Spherical sector

Here we evaluate the axial demagnetization factor of the spherical sector, starting from Eq. (44). Similarly to the hemispherical case in Appendix B.1, the integration along x annihilates all m terms except when $m \in \{n-2, n, n+2\}$. Using Eq. (B.2) to integrate the remaining terms, we find that

$$\begin{aligned}N_z(x_0) = \frac{1}{V}\sum_{n=0}^\infty p_n(x_0)\int_0^\infty k^2\mathrm{d}k F_n^2(k) \\ - \frac{2}{V}\sum_{n=0}^\infty q_n(x_0)\int_0^\infty k^2\mathrm{d}k F_n(k)F_{n+2}(k)\end{aligned} \tag{B.13}$$

where

$$p_n(x_0) = a_n^2(x_0)\frac{2(2n^2+2n-1)}{(2n-1)(2n+1)(2n+3)} \tag{B.14}$$

$$q_n(x_0) = a_n(x_0)a_{n+2}(x_0)\frac{2(n+1)(n+2)}{(2n+1)(2n+3)(2n+5)} \tag{B.15}$$

Referring to Appendix B.1, and substituting $\ell \to (n+1)/2$ in the appropriate equations, the radial integrals are seen to be

$$\int_0^\infty k^2\mathrm{d}k F_n^2(k) = \frac{\pi R^3}{6} \tag{B.16}$$

and

$$\int_0^\infty k^2\mathrm{d}k F_n(k)F_{n+2}(k) = \frac{\pi}{6}R^3\frac{n}{n+3} \tag{B.17}$$

Considering that $V = (2/3)\pi R^3(1-x_0)$, we finally acquire Eq. (45).

B.3. Spherical cap

Here, we evaluate Eq. (46) to determine the in-plane demagnetization factor of the spherical cap, where as noted in Section 4.3 the only charge is $\sigma_m = M_0 \sin\theta\cos\phi$ on the curved top, so Eq. (46) reduces to a surface integral. The cap volume equals the volume of the corresponding spherical sector, minus the conical part:

$$\begin{aligned}V_{\mathrm{cap}} &= 2\pi\int_0^{\theta_0}\sin\theta\mathrm{d}\theta\int_0^R r^2\mathrm{d}r - \frac{\pi}{3}R^3\sin^2\theta_0\cos\theta_0 \\ &= \frac{\pi}{3}R^3(1-x_0)^2(2+x_0)\end{aligned} \tag{B.18}$$

hence

$$N_x = \frac{3}{2(1-x_0)^2(2+x_0)}\sum_{\ell=1}^\infty \gamma_\ell(x_0)\int_{x_0}^1 \sqrt{1-x^2}P_\ell^1(x)\mathrm{d}x, \tag{B.19}$$

where we already did the azimuthal integral. For the remaining, polar integral we can combine Eqs. (32) and (A.23), yielding

$$\int_{x_0}^1 \sqrt{1-x^2}P_\ell^1(x)\mathrm{d}x = \ell(\ell+1)\gamma_\ell(x_0), \tag{B.20}$$

so that N_x is given by Eq. (47).

The hemisphere is a special case of the spherical cap where $\theta_0 = \pi/2$. Thus for $x_0 = 0$, Eq. (47) should reproduce the demag factors of a hemisphere. Using that

$$P_{2n}(0) = (-1)^n\frac{(2n-1)!!}{(2n)!!} \quad , \quad P_{2n+1}(0) = 0 \tag{B.21}$$

Eq. (39) reduces to $\gamma_{2n+1}(0) = 0$ for $n \geq 1$ while $\gamma_1(0) = -1/3$ and

$$\gamma_{2n}(0) = (-1)^n\frac{(2n-3)!!}{(2n+2)!!} = \frac{\Gamma\left(n-\frac{1}{2}\right)}{4\sqrt{\pi}\Gamma(n+2)}, \tag{B.22}$$

hence, we may write

$$N_x(0) = \frac{1}{6} + \frac{3}{32\pi}\sum_{n=1}^\infty n(2n+1)\frac{\Gamma\left(n-\frac{1}{2}\right)^2}{\Gamma(n+2)^2}. \tag{B.23}$$

As may be verified by a computer algebra system such as Maple, the exact value of the sum is $N_x(0) = 7/(9\pi)$, in agreement with the shape amplitude calculation.

Data availability

No data was used for the research described in the article.

References

[1] R. Bjørk, E. Poulsen, K. Nielsen, A. Insinga, MagTense: A micromagnetic framework using the analytical demagnetization tensor, J. Magn. Magn. Mater. 535 (2021) 168057, http://dx.doi.org/10.1016/j.jmmm.2021.168057, URL https://linkinghub.elsevier.com/retrieve/pii/S0304885321003334.

[2] K.K. Nielsen, A.R. Insinga, R. Bjork, The stray and demagnetizing field of a homogeneously magnetized tetrahedron, IEEE Magn. Lett. 10 (2019) 1–5, http://dx.doi.org/10.1109/LMAG.2019.2956895, URL https://ieeexplore.ieee.org/document/8918242/.

[3] A.P. Guimaraes, Principles of Nanomagnetism, Springer-Verlag, Berlin, Heidenberg, 2009.

[4] J. Philip, Magnetic nanofluids (ferrofluids): Recent advances, applications, challenges, and future directions, Adv. Colloid Interface Sci. 311 (2023) 102810.

[5] G.-P. Zhu, N.-T. Nguyen, R.V. Ramanujan, X.-Y. Huang, Nonlinear deformation of a ferrofluid droplet in a uniform magnetic field, Langmuir 27 (24) (2011) 14834–14841, http://dx.doi.org/10.1021/la203931q, URL https://pubs.acs.org/doi/10.1021/la203931q.

[6] G.-P. Zhu, S.-H. Wu, S.-Z. Zheng, L. Li, N.-T. Nguyen, Investigation of ferrofluid sessile droplet tensile deformation in a uniform magnetic field, Magnetochemistry 9 (10) (2023) 215, http://dx.doi.org/10.3390/magnetochemistry9100215, URL https://www.mdpi.com/2312-7481/9/10/215.

[7] A. Khan, S.-T. Zhang, Q.-P. Li, H. Zhang, Y.-Q. Wang, X.-D. Niu, Wetting dynamics of a sessile ferrofluid droplet on solid substrates with different wettabilities, Phys. Fluids 33 (4) (2021) 042115, http://dx.doi.org/10.1063/5.0047553, URL https://pubs.aip.org/pof/article/33/4/042115/1064236/Wetting-dynamics-of-a-sessile-ferrofluid-droplet.

[8] E.C. Stoner, XCVII. the demagnetizing factors for ellipsoids, Lond. Edinb. Dublin Philos. Mag. J. Sci. 36 (263) (1945) 803–821, http://dx.doi.org/10.1080/14786444508521510, URL http://www.tandfonline.com/doi/abs/10.1080/14786444508521510.

[9] J.A. Osborn, Demagnetizing factors of the general ellipsoid, Phys. Rev. 67 (11–12) (1945) 351–357, http://dx.doi.org/10.1103/PhysRev.67.351, URL https://link.aps.org/doi/10.1103/PhysRev.67.351.

[10] P. Rhodes, Demagnetising energies of uniformly magnetised rectangular blocks, Proc. Leeds Phil. Liter. Soc. 6 (1954) 191–210.

[11] A. Aharoni, Introduction to the Theory of Ferromagnetism, vol. 109, Clarendon Press, 2000.

[12] G. Rowlands, Demagnetising Energies and Domain Structures in Ferromagnetics (Ph.D. thesis), University of Leeds (Physics Department), 1956.

[13] G. Rowlands, On the calculation of acoustic radiation impedance of polygonal-shaped apertures, J. Acoust. Soc. Am. 92 (5) (1992) 2961–2963, http://dx.doi.org/10.1121/1.404360, URL https://pubs.aip.org/jasa/article/92/5/2961/843669/On-the-calculation-of-acoustic-radiation-impedance.

[14] W.F. Brown, 1904-1983 magnetostatic principles in ferromagnetism, in: Series of Monographs on Selected Topics in Solid State Physics; v. 1, North-Holland Pub. Co.; Interscience Publishers, Amsterdam, New York, 1962, URL http://catalog.hathitrust.org/api/volumes/oclc/1894084.html.

[15] R.I. Joseph, Ballistic demagnetizing factor in uniformly magnetized cylinders, J. Appl. Phys. 37 (13) (1966) 4639–4643.

[16] D.-X. Chen, J. Brug, R. Goldfarb, Demagnetizing factors for cylinders, IEEE Trans. Magn. 27 (4) (1991) 3601–3619, http://dx.doi.org/10.1109/20.102932, URL https://ieeexplore.ieee.org/document/102932/.

[17] Y.T. Millev, E. Vedmedenko, H.P. Oepen, Dipolar magnetic anisotropy energy of laterally confined ultrathin ferromagnets: Multiplicative separation of discrete and continuum contributions, J. Phys. D: Appl. Phys. 36 (23) (2003) 2945–2949, http://dx.doi.org/10.1088/0022-3727/36/23/012, URL https://iopscience.iop.org/article/10.1088/0022-3727/36/23/012.

[18] A. Hubert, R. Schäfer, Magnetic Domains the Analysis of Magnetic Microstructures, Springer, Berlin, 1998, http://dx.doi.org/10.1007/978-3-540-85054-0, URL https://archive.org/details/magneticdomainsa0000hube.

[19] M. Beleggia, M. De Graef, On the computation of the demagnetization tensor field for an arbitrary particle shape using a Fourier space approach, J. Magn. Magn. Mater. 263 (1–2) (2003) L1–L9, http://dx.doi.org/10.1016/S0304-8853(03)00238-5, URL https://linkinghub.elsevier.com/retrieve/pii/S0304885303002385.

[20] M. Beleggia, M. De Graef, General magnetostatic shape–shape interactions, J. Magn. Magn. Mater. 285 (1) (2005) L1–L10, http://dx.doi.org/10.1016/j.jmmm.2004.09.004, URL https://www.sciencedirect.com/science/article/pii/S0304885304008923.

[21] M. Beleggia, M.D. Graef, Y.T. Millev, D.A. Goode, G. Rowlands, Demagnetization factors for elliptic cylinders, J. Phys. D: Appl. Phys. 38 (18) (2005) 3333, http://dx.doi.org/10.1088/0022-3727/38/18/001.

[22] M. Beleggia, M. De Graef, Y.T. Millev, Magnetostatics of the uniformly polarized torus, Proc. R. Soc. A: Math. Phys. Eng. Sci. 465 (2112) (2009) 3581–3604, http://dx.doi.org/10.1098/rspa.2009.0355, URL https://royalsocietypublishing.org/doi/10.1098/rspa.2009.0355.

[23] M. Beleggia, J. Lau, M. Schofield, Y. Zhu, S. Tandon, M. De Graef, Phase diagram for magnetic nano-rings, J. Magn. Magn. Mater. 301 (1) (2006) 131–146, http://dx.doi.org/10.1016/j.jmmm.2005.06.024, URL https://linkinghub.elsevier.com/retrieve/pii/S0304885305006554.

[24] M. Beleggia, D. Vokoun, M. De Graef, Demagnetization factors for cylindrical shells and related shapes, J. Magn. Magn. Mater. 321 (9) (2009) 1306–1315, http://dx.doi.org/10.1016/j.jmmm.2008.11.046, URL https://linkinghub.elsevier.com/retrieve/pii/S0304885308011682.

[25] M. Beleggia, M. De Graef, Y. Millev, Demagnetization factors of the general ellipsoid: an alternative to the Maxwell approach, Phil. Mag. 86 (16) (2006) 2451–2466, http://dx.doi.org/10.1080/14786430600617161, URL https://www.tandfonline.com/doi/abs/10.1080/14786430600617161.

[26] R. Streubel, P. Fischer, F. Kronast, V.P. Kravchuk, D.D. Sheka, Y. Gaididei, O.G. Schmidt, D. Makarov, Magnetism in curved geometries, J. Phys. D: Appl. Phys. 49 (36) (2016) 363001, http://dx.doi.org/10.1088/0022-3727/49/36/363001, URL https://iopscience.iop.org/article/10.1088/0022-3727/49/36/363001.

[27] E. Berganza, J.A. Fernandez-Roldan, M. Jaafar, A. Asenjo, K. Guslienko, O. Chubykalo-Fesenko, 3D quasi-skyrmions in thick cylindrical and dome-shape soft nanodots, Sci. Rep. 12 (1) (2022) 3426, http://dx.doi.org/10.1038/s41598-022-07407-w, URL https://www.nature.com/articles/s41598-022-07407-w.

[28] P. Johnson, A.K. Gangopadhyay, R. Kalyanaraman, Z. Nussinov, Demagnetization-Borne microscale skyrmions, Phys. Rev. B 86 (6) (2012) 064427, http://dx.doi.org/10.1103/PhysRevB.86.064427, URL https://link.aps.org/doi/10.1103/PhysRevB.86.064427.

[29] M. Beleggia, S. Tandon, Y. Zhu, M. De Graef, On the magnetostatic interactions between nanoparticles of arbitrary shape, J. Magn. Magn. Mater. 278 (1–2) (2004) 270–284, http://dx.doi.org/10.1016/j.jmmm.2003.12.1314, URL https://linkinghub.elsevier.com/retrieve/pii/S0304885304000186.

[30] S. Blundell, Magnetism in Condensed Matter, First Ed., Oxford University Press, 2001.

[31] D.J. Griffiths, Introduction to Electrodynamics, Fourth ed., Pearson, Boston, 2013.

[32] G.B. Arfken, H.-J. Weber, Mathematical Methods for Physicists, fifth ed., Harcourt/Academic Press, San Diego, 2001.

[33] R. Mehrem, The plane wave expansion, infinite integrals and identities involving spherical bessel functions, Appl. Math. Comput. 217 (12) (2011) 5360–5365, http://dx.doi.org/10.1016/j.amc.2010.12.004, URL https://linkinghub.elsevier.com/retrieve/pii/S0096300310011914.

[34] G.N. Watson, A treatise on the theory of Bessel functions, in: Cambridge Mathematical Library, second ed., Cambridge University Press, Cambridge [England] ; New York, 1944.

[35] L. Infeld, T.E. Hull, The factorization method, Rev. Modern Phys. 23 (1) (1951) 21–68, http://dx.doi.org/10.1103/RevModPhys.23.21, URL https://link.aps.org/doi/10.1103/RevModPhys.23.21.

[36] J.D. Jackson, Classical Electrodynamics, Third ed., American Association of Physics Teachers, 1999.